Journal of the European Ceramic Society **9** (1992) 133–142

Crack Tip Bridging Stresses in Alumina and Duplex Ceramics

H. E. Lutz, X. Z. Hu* & M. V. Swain

Center for Advanced Materials Technology, Department of Mechanical Engineering, University of Sydney, NSW 2006, Australia

(Received 1 May 1991; accepted 20 June 1991)

Abstract

Crack tip bridging stresses in three alumina and three duplex ceramics are evaluated with a simple bridging theory, which utilizes the difference in compliance predicted for a crack of known size and that measured. The crack growth resistance (R-curve) behaviour of these ceramic materials is clearly elucidated by the bridging stresses evaluated. In addition, a consecutive cutting technique developed for cementitious materials is adopted to progressively remove the crack-wake bridging zone in two of these duplex ceramics. Variation in the unloading compliance and the crack growth resistance during consecutive cutting is observed, which provides further evidence of the predominant contribution of crack-wake bridging to the R-curve behaviour of these ceramic materials. The values obtained for the magnitude and range of the bridging stresses calculated using this approach are very similar to those recently calculated for alumina from direct scanning electron measurements of crack opening displacement of the crack tip.

Für drei Al_2O_3-Werkstoffe und drei Verbundwerkstoffe wurden mittels einer einfachen Brückentheorie die Rißüberbrückungsspannungen hinter der Rißspitze untersucht. Diese Theorie basiert dabei auf dem Unterschied zwischen der gemessenen und der für einen Riß mit bekannter Länge vorausgesagten elastischen Nachgiebigkeit. Das R-Kurvenverhalten dieser keramischen Materialien kann eindeutig durch die berechneten Rißüberbrückungsspannungen erklärt werden. Zusätzlich wurde für zwei der Verbundwerkstoffe eine ursprünglich für Zement entwickelte Sägemethode angewandt, bei der fortlaufend die Rißüberbrückungszone entfernt wird. Die beim fortlaufenden Nachsägen beobachtete Veränderung der elastischen Nachgiebigkeit beim Entlasten sowie der Rißwiderstandskurve sind ein weiterer Beweis dafür, daß das R-Kurvenverhalten dieser Werkstoffe hauptsächlich durch Rißüberbrückung hinter der Rißspitze verursacht wird. Die mit diesem Verfahren berechneten Werte der Rißüberbrückungsspannungen stimmen mit kürzlich an Al_2O_3 mittels rasterelektronenmikroskopischer Vermessung der Rißöffnung an der Rißspitze berechneter Werte relativ gut überein.

On évalue les tensions pontales en front de fissure pour trois alumines et trois céramiques duplex par une théorie de pontage simple, qui utilise la différence, pour une fissure de taille connue, entre la valeur de compliance prévue et celle mesurée. Le comportement de ces céramiques vis à vis de la résistance à la croissance de la fissure (courbe R) est bien expliqué par les contraintes pontales ainsi évaluées. Dans deux des céramiques duplex, on utilise de plus une technique d'entaillage, développée pour les matériaux cémentés, afin de supprimer progressivement la zone pontale correspondant au sillage de la fissure. On observe des variations de compliance dans la phase décroissante de la charge ainsi que des variations de résistance à la croissance de la fissure pendant l'entaillage, ce qui montre la contribution prédominante de la zone pontale à la courbe R. Les valeurs obtenues, concernant l'importance aussi bien que l'éventail des tensions pontales, calculées en utilisant cette approche, sont très similaires à celles récemment calculées pour l'alumine à partir de mesures directes en balayage électronique du déplacement de l'ouverture de la fissure, en front de fissure.

* Present address: Department of Mechanical Engineering, University of Western Australia, WA 6009, Australia.

Journal of the European Ceramic Society 0955-2219/92/$5.00

1 Introduction

An increasing crack resistance or toughness during crack extension, namely R-curve or K^R-curve behaviour, is a direct consequence of energy-dissipating toughening mechanisms which reduce the crack driving force at the crack tip.[1,2] One of the first documentations of this phenomenon was made by Hübner & Jillek.[3] In the following years further studies have confirmed that toughening mechanisms in the crack-wake region are mainly responsible for the increasing crack growth resistance.[4] R-Curves have been observed in a wide range of ceramics.[4-8] Although there is no unique R-curve for a material,[4,9,10] i.e. the R-curve depends on the initial crack length, specimen geometry and dimensions and testing conditions, it provides a more satisfactory explanation of the fracture behaviour of toughened ceramic materials than the assumption of constant K_{Ic}. Rising R-curves have been observed for coarse-grained ceramics with thermal expansion anisotropy[3,4] and for transformation toughened ceramics.[5] However, for brittle linear–elastic materials, such as glass and most fine-grained ceramics, it is expected that the fracture toughness is constant and independent of crack extension.

The toughening mechanisms can be subdivided into[2]

(1) crack deflection and crack branching;[11-13]
(2) contact shielding processes: wedging caused by broken-out grains or rough crack surfaces,[4] and crack bridging;[5,11,13]
(3) zone shielding processes (stress-induced): transformation and microcracking[9,11,13-15] and residual stress fields.[8,10,11,13]

It is difficult to estimate the contribution of a specific single mechanism to K^R from experimental data. On the one hand not all toughening effects can be visualized, and on the other hand they seldom appear singly. Toughening mechanisms which are activated by stresses caused by thermal expansion mismatch or phase transformation are temperature sensitive and, hence, so is their contribution to K^R. The work of Steinbrech and coworkers[16,17] has convincingly demonstrated the importance of crack bridging to the toughness of ceramics. Their work was novel in that it conclusively showed that so-called 'damage' or microcracking process zones ahead of the crack tip were far less effective than had been believed.

One of the problems currently existing in the field of crack tip bridging is the means to simply and reliably estimate the magnitude of these stresses. Mai & Lawn[18] were one of the first groups to propose a simple power law to fit the form of the stress distribution over the bridging zone. On the basis of this and other simplifying assumptions they were able to fit such functions to the measured R-curve behaviour. Much of this approach was an extension of concepts[19,20] for fibre-reinforced cementitious materials. These authors also pointed out the importance of crack opening angle associated with different testing geometries (single-edge notched bend (SENB) or double cantilever beam (DCB)) to the slope of the R-curves measured. Steinbrech *et al.*[17] have recently utilized such methodology to reinterpret their R-curve observations and their dependence upon crack length to specimen width (a/W) ratio. The importance of specimen geometry may be readily appreciated by comparing the SENB observations of R-curve behaviour by Knehans & Steinbrech[16] to that of DCB measurements by Swain[21] on the same materials.

More recently Hu & Wittmann[22-25] introduced a novel technique based on the double-notching method of Knehans & Steinbrech[16] for the determination of crack bridging in mortar and concrete. This consisted of serial re-notching of an extended crack of length a to a depth Δa from the initial notch length a_0 and measuring the change in compliance, $C_u(\Delta a)$, after each renotching step, as shown in Fig. 1. The $C_u(\Delta a)$ curve starts with the value $C_u(a)$, increases gradually as the bridging zone is removed, and reaches a value $C(a)$ when the original crack is completely renotched. This value equals the compliance of an ideal linear–elastic-behaving specimen with an extended crack or notch of length a. The exact value can be calculated from a calibration

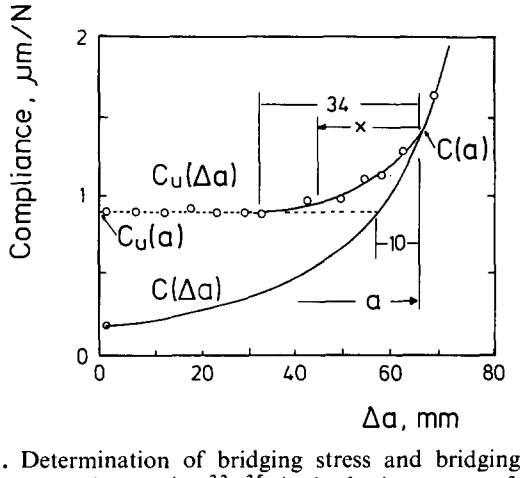

Fig. 1. Determination of bridging stress and bridging zone from consecutive cutting.[22-25] Δa is the increment of notch length ($\Delta a = 0$ at the initial notch tip). $C_u(\Delta a)$ increases as bridging stresses are removed. $C_u(\Delta a) = C(\Delta a)$ if the bridging zone is cut through.

function (Section 3). Since it is very difficult to measure the crack length in mortar and concretes, $C(a)$ can not be calculated. A better method to determine both a and $C(a)$ simultaneously is by comparing $C_u(\Delta a)$ with the compliance curve $C(\Delta a)$ which would be obtained by notching an uncracked linear–elastic-behaving material in the same way. $C(\Delta a)$ can be easily calculated (Section 3). Both curves will intersect when the notch is extended to a. In this way it is also possible to determine the extent of the crack tip bridging zone as well as the bridging stress distribution. The compliance analysis[22–24] originally developed to calculate the bridging stress from the compliance variation has been further extended so that bridging stresses can be evaluated without re-notching.[26] Such an extension is particularly useful for ceramic materials as often the extent of crack growth before saturation of a R-curve is small. This approach has been successfully applied to two ceramic materials in a previous work.[27]

In the present paper, the simplified approach and the consecutive cutting technique[22–25] are applied to various ceramic materials. Experimental results on the R-curve behaviour and bridging stresses of three alumina ceramics of different grain size (tested by Swain[21] and Lutz & Swain[28]), two alumina-based duplex ceramics and a duplex ceramic showing the extraordinary effect of a crack-branching chain reaction are presented. The duplex ceramics have been fabricated and tested by Lutz and coworkers.[13,28] In addition, two samples of the alumina-based duplex ceramics with extended cracks are renotched progressively, as in Fig. 1. In one case an attempt was made to measure the reduction in K^R generating a 'negative' K^R-curve.

2 Basic Bridging Stress Formulae

As shown in Fig. 2(a), the major material properties concerned with a bridged crack a are the length of the bridging zone X, the critical crack opening w_c, the maximum bridging stress σ_m and the form of bridging stress distribution. Normally, the magnitude of the bridging stress σ_b is determined by the crack opening w. The area under the σ_b–w curve, Fig. 2(b), is defined as the specific fracture energy G_f.

Following previous work[18,20] the authors have used a simple power-law function to describe bridging stresses in a ceramic material, namely

$$\frac{\sigma_b}{\sigma_m} = \left[1 - \frac{w}{w_c}\right]^n \tag{1}$$

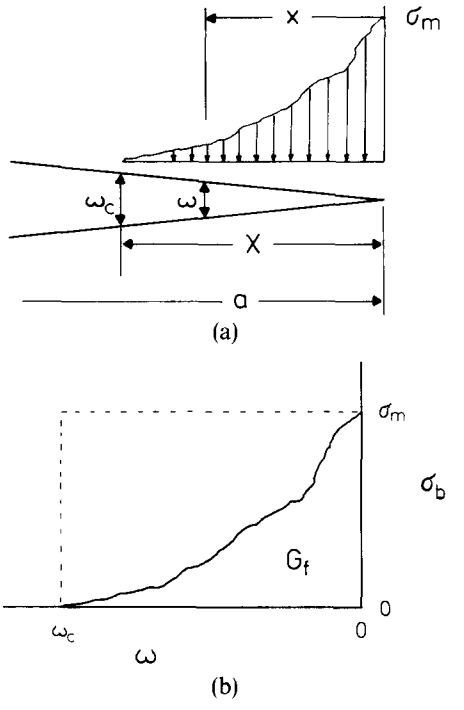

Fig. 2. (a) Bridging stress and bridged crack a in quasi-brittle material, (b) σ_b–w relationship and fracture energy G_f.

This function is illustrated in Fig. 3 for various n values representing materials from ideal linear–elastic ($n = \infty$) to perfect elastic–plastic ($n = 0$). From the power-law function G_f is given by:

$$G_f = \int_0^{w_c} \sigma_b \, dw = \frac{\sigma_m w_c}{n+1} \tag{2}$$

The fracture energy can also be related to the crack growth resistance curve of a ceramic material. Let K_{ic} denote the initial value of a K^R-curve and K_∞ represent the steady-state value. Hence,

$$G_f = \frac{1-\nu^2}{E} \cdot (K_\infty^2 - K_{ic}^2) \tag{3}$$

where E is Young's modulus and ν the Poisson ratio.

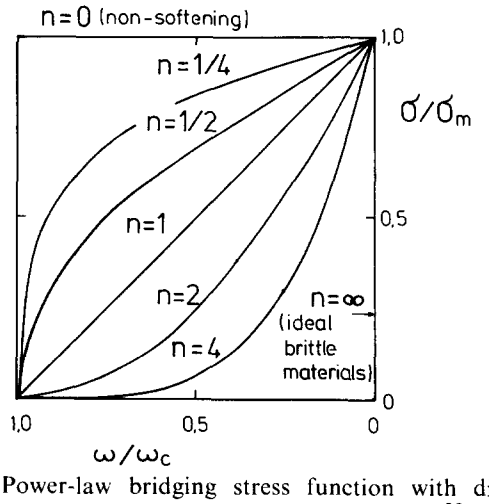

Fig. 3. Power-law bridging stress function with different exponents representing various materials.[20]

For an extended crack a, a corresponding unloading compliance $C_u(a)$ can be measured. As the bridging stresses behind the crack tip a resist crack opening and thus influence $C_u(a)$, the ideal linear-elastic compliance $C(a)$ is different from $C_u(a)$ as shown in Fig. 1. In general, $C(a) > C_u(a)$ if bridging is the major toughening mechanism. As full details for the compliance analysis on $C(a)$ and $C_u(a)$ have been given in previous works[22-24] and the further simplified analysis can be found in Refs 26 and 27 only basic formulae concerning bridging stress evaluation are given in this section. However, some illustrative derivations are given in the Appendix.

If a steady-state bridging zone X is established behind a crack tip a, the theoretical compliance $C(a)$ and measured $C_u(a)$ can be related to the fracture energy G_f and other bridging stress parameters[22-24] by

$$\frac{C(a)}{C'(a)} \cdot \left\{ \frac{C(a)}{C_u(a)} - 1 \right\} = X \cdot \frac{G_f}{\sigma_m w_c} \tag{4}$$

The relationship between $C(a)$ and $C_u(a)$ before the saturation of the bridging zone has also been established.[22-24] Using the power-law bridging stress function defined in eqn (1), it can be shown that:

$$\phi = \frac{C(a)}{C'(a)} \cdot \left\{ \frac{C(a)}{C_u(a)} - 1 \right\} = \begin{cases} \dfrac{X}{n+1} & \Delta a > X \\ \dfrac{X}{n+1} \cdot \left\{ 1 - \left[1 - \dfrac{\Delta a}{X} \right]^{n+1} \right\} & \Delta a < X \end{cases} \tag{5}$$

Let a_0 be the initial crack length and $\Delta a = a - a_0$, i.e. the crack extension. With the measured crack length a and compliance $C_u(a)$, the compliance ϕ-function can be evaluated. The exponent n of the power-law bridging stress distribution and the steady-state bridging zone X can then be determined with the ϕ-curve.

3 Experimental Procedure

The present work was carried out on:

(1) Alumina ceramics with grain sizes 1, 16 and 25 μm. The 1 μm alumina material was fabricated and tested by Lutz & Swain.[28] Its toughness curve with crack growth was measured with a compact tension (CT) sample of width $W = 21{\cdot}05$ mm, initial crack length $a_0 = 12{\cdot}00$ mm and thickness $b = 3{\cdot}20$ mm. The 16 μm alumina was supplied by Steinbrech and tested by Swain.[21] The grain structure of the material appeared equiaxed with the average grain size D_A about 16 μm, although the occasional grain up to 60 μm could be seen. A DCB sample of dimensions ~ 3·3 mm × 14·2 mm × 80 mm was used. A guide notch was introduced along one side of the specimen. The crack was propagated from a 200 μm wide prenotch with a length of 19 mm. The third alumina ceramic had a somewhat more acicular structure with an average grain size of 25 μm. The K^R-curve was measured by Lutz & Swain.[28] The test was carried out on a CT sample with $W = 30{\cdot}10$ mm, $a_0 = 18{\cdot}00$ mm and $b = 3{\cdot}70$ mm.

(2) Two duplex ceramics with an alumina matrix (CT 8000 SG; Alcoa, Bauxite, USA) (1 μm alumina as in (1)) and one duplex ceramic with a matrix consisting of 3Y-TZP (3 mol% yttria-containing tetragonal zirconia polycrystals) plus 20 wt% of Al_2O_3 (TZ-3Y20A; Tosoh Corp., Tokyo, Japan). The two alumina-based duplex ceramics contained 10 vol.% of pressure zones having diameters of 16–32 μm. The pressure zones consisted of Al_2O_3 (CT 8000 SG; Alcoa) + 35 vol.% monoclinic (m-) ZrO_2 (Dynazirkon F; Dynamit Nobel, Bristol, PA) in the one material and Al_2O_3 + 50 vol.% m-ZrO_2 in the other material. For further considerations the former material is labeled 2, the latter 3, and their alumina matrix 1. CT samples were prepared for materials 2 and 3 with the dimensions $W = 21{\cdot}05$ mm, $a_0 = 12{\cdot}00$ mm and $b = 2{\cdot}95$–$3{\cdot}20$ mm, and were tested by Lutz & Swain.[28]

The TZP–alumina-based duplex ceramic was prepared and tested by Lutz and coworker.[13,29-31] The material contained 20 vol.% of pressure zones. The pressure zones consisted of equal volumes of Al_2O_3 and m-ZrO_2 and had 45–65 μm diameter. The method of the fabrication of duplex ceramics and their components has been described in detail in a previous paper.[29] The CT sample had the dimensions $W = 21{\cdot}60$ mm, $a_0 = 6{\cdot}48$ mm and $b = 3{\cdot}17$ mm.

The crack propagation in all the ceramic materials was measured directly using a traveling microscope. The crack opening displacement was obtained from a strain gauge based clip gauge attached to the test pieces. For the CT sample geometry the K^R-values were calculated on the basis of the load P, the

relative crack length a/W, the sample thickness b and the appropriate Y-function, namely,[32]

$$K^R = Y(a/W)\frac{P}{bW^{1/2}} \tag{6}$$

for $a/W \leq 0{\cdot}85$ with

$$Y(a/W) = \frac{(2 + a/W)}{(1 - a/W)^{3/2}}[0{\cdot}886 + 4{\cdot}64(a/W) - 13{\cdot}32(a/W)^2 + 14{\cdot}72(a/W)^3 - 5{\cdot}6(a/W)^4] \tag{7}$$

For the DCB geometry the value of the stress-intensity factor was calculated from the analysis of Freiman *et al.*, namely,[33]

$$K = \frac{Pa}{It^2}[(1 + \lambda/a)^2 + 0{\cdot}41(h/a)^2]^{1/2} \tag{8}$$

where P is the applied load, a the crack length, I the moment of inertia, h the beam height, t the thickness of web section and λ a constant to account for the width of the guide notch.

During the experiment, an unloading/reloading cycle was conducted for every crack measurement, to determine the compliance $C_u(a)$ used in eqn (5). Some hysteresis with this unloading/reloading cycle was noted. All estimates of specimen compliance were made during unloading. The compliance $C(a)$ without bridging influence was calculated with the crack measurement for DCB and CT specimens. That is:

$$C(a) = \frac{4}{E^* t}\cdot\left(\frac{a}{h}\right)^3\left(1 + 0{\cdot}64\frac{h}{a}\right)^3 \tag{9}$$

for DCB specimens,[34] and

$$C(a) = \frac{1}{E^* t}\cdot\left(1 + \frac{0{\cdot}25}{\alpha}\right)\left(\frac{1+\alpha}{1-\alpha}\right)^2\cdot (1{\cdot}6137 + 12{\cdot}678\alpha - 14{\cdot}231\alpha^2 - 16{\cdot}610\alpha^3 + 35.050\alpha^4 - 14{\cdot}494\alpha^5) \tag{10}$$

for CT specimens[35] (where $\alpha = a/W$). E^* was determined from the initial slope of a load/displacement curve with a_0 being substituted into the above equations.

With the measurements of load and crack length (P,a), K_R-curves were calculated from the above equations. In addition, with the measurements of compliance and crack length (C_u,a), ϕ-curves were evaluated through eqn (5).

In two additional experiments, the samples of the alumina-based duplex ceramics 2 and 3 with extended cracks were renotched progressively as in Fig. 1. The change in compliance, $C_u(\Delta a)$, was measured for various recutting distances Δa and compared with the compliance $C(\Delta a)$ expected for recutting an uncracked ideal linear–elastic-behaving material. In the case of material 2, the change of K^R was measured. This was performed after every recutting step by loading the sample carefully to the critical load to initiate crack propagation, then rapidly unloading the sample to keep the crack extension as small as possible ($< 50\,\mu m$).

4 Results and Discussion

After the determination of K^R- and ϕ-curves, the bridging stress parameters may now be estimated with the equations given in Section 2. The saturated bridging zone X can be determined equally well from either the K^R- or ϕ-curve, or from the consecutive cutting results as shown in Fig. 1. Based on the linear crack profile assumption, the critical crack opening displacement w_c for a standard CT specimen is given by:

$$w_c = \delta_{CMOD}\cdot\frac{X}{a + 0{\cdot}25W} \tag{11}$$

where δ_{CMOD} is the crack mouth opening displacement. Bridging stress parameters estimated for various ceramics tested are summarized in Table 1. Bridging stress distributions indicated by the exponents n listed in Table 1 can be best understood from Fig. 3.

The K^R-curves of alumina ceramics with different grain size are shown in Fig. 4 and the corresponding

Table 1. Bridging stress parameters

	Al_2O_3			*Material 2*	*Material 3*	*Material 4*
	1 μm	*16 μm*	*25 μm*			
X (mm)	1·55	8	8	3	4	9
w_c (μm)	1	4[a]	23	3·8	8·1	33
n	3·7	2·1	0·9	~2	~0	0·7
σ_m (MPa)	52	56	15	120	56	24
G_f (N/m)	11	72	178	134	452	474

[a] Measured by Steinbrech *et al.*[17]

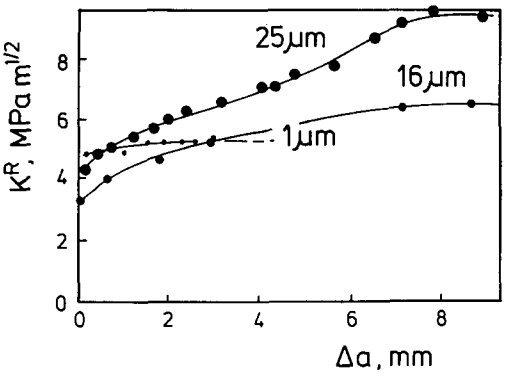

Fig. 4. Crack growth resistance curves of alumina ceramics. $\Delta a (= a - a_0)$ indicates crack growth. CT samples were used for the 1 μm and 25 μm alumina ceramics and DCB specimens for the 16 μm alumina.

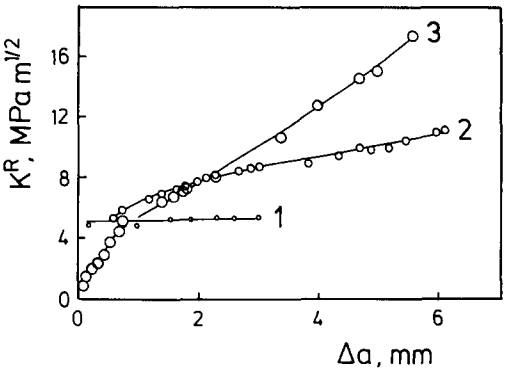

Fig. 6. K^R-curves of two alumina-based duplex ceramics (materials 2 and 3) and their pure alumina matrix (1 μm grain size) (material 1). Again, Δa indicates crack growth. CT samples were used for all materials.

ϕ-curves in Fig. 5. The ϕ-curves indicate only the toughness increment due to bridging, while the K^R-curves show the overall toughness. Therefore, a higher steady-state ϕ-value implies a more pronounced K^R-curve. This is also reflected by n, σ_m and G_f of these alumina ceramics given in Table 1. The initial negative ϕ-values in Fig. 5 seem to be due to numerical errors. They are very close to zero. It should be mentioned that CT specimens were used to obtain the results shown in Figs 4 and 5 except for those of the 16 μm alumina obtained with a DCB sample.[21] The results of $n \approx 2{\cdot}1$ and $\sigma_m = 56$ MPa obtained for the 16 μm alumina is comparable to those determined by Steinbrech *et al.*[17] for the same alumina ($n = 2$, 3, 4, and $\sigma_m = 33$, 46, 60 MPa), and the results of $n = 2{\cdot}5$ and $\sigma_m = 70$ MPa obtained by Rödel *et al.*[36] from in-situ scanning electron microscope (SEM) measurements of bridged crack interfaces for an alumina with the average grain size D_A of 11 μm. In general, it is expected that X, w_c and G_f of alumina increase, whereas n and σ_m decrease with increasing grain size, due to increasing bridging stresses.

The results of the 1 μm alumina are also shown in Figs 6 and 7 as a comparison to the alumina-based duplex ceramics. The feature that a high steady-state ϕ-value indicates a pronounced K^R-curve is also confirmed by these duplex ceramics. It is noted that the ϕ-curves of the 25 μm alumina in Fig. 5 and material 3 in Fig. 7 are similar.

It is obvious that bridging is the predominant toughening mechanism for the coarser-grained alumina ceramics shown in Figs 4 and 5, and the alumina-based duplex ceramics in Figs 6 and 7. The virtual absence of negative ϕ-values for the alumina materials confirms recent predictions by Lawn[37] of the lack of any substantive microcrack zone about a crack tip of alumina of fine to medium (50 μm) grain size.

The load–displacement and the K^R-curve behaviour of the TZP–alumina duplex ceramic (material 4) are illustrated in a recent paper by Lutz *et al.*[13] A crack-branching chain reaction develops during the K^R-curve test, resulting in a crack network of considerable size. The development of this unusual effect is documented by a photograph series taken *in situ*.[13] With the crack approaching the rear side of the specimen after a propagation of c.

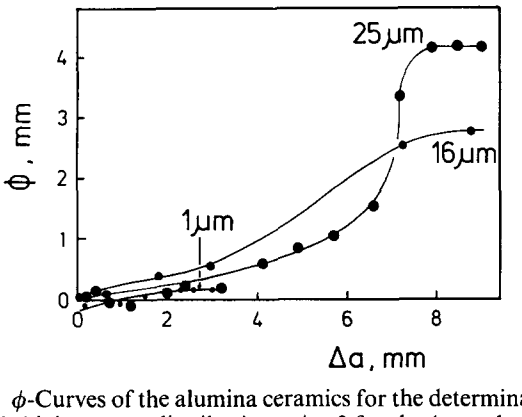

Fig. 5. ϕ-Curves of the alumina ceramics for the determination of the bridging stress distributions. $\phi \sim 0$ for the 1 μm alumina, indicating that there is little bridging influence.

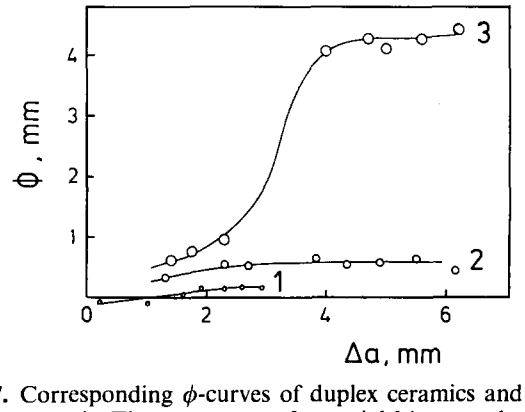

Fig. 7. Corresponding ϕ-curves of duplex ceramics and 1 μm alumina matrix. The exponent n of material 3 is around zero as $X/(n+1) \sim X$.

10–12 mm ($a/W = 0{\cdot}76$–$0{\cdot}86$), its propagation is slowed down, whereas the damage zone expands further, perpendicular to the crack propagation direction and even back to the notch region. The load required to open the crack mouth and to further extend the crack decreased only gradually when compared to a considerable load decrease observed in brittle materials. For the main crack length exceeding 14 mm, corresponding to a a/W value of more than 0·95, the specimen could still be loaded by 50 N without causing any visible damage or crack extension. It is thought that this load is necessary to overcome frictional stresses in the damage zone. Inserting this value into eqn (7) gives a Y-function value of 351 and with eqn (6) a K^R-value of 38 MPam$^{1/2}$. Due to the high load necessary to open the crack, which decreased only slowly with increasing crack extension, the K^R-curve follows almost the same steep increase as the Y-function. This is thought to be an artificial effect which is, however, an indicator of the presence of bridging stresses.

Both the K^R- and ϕ-curves of the duplex ceramic shown in Fig. 8 are very similar in shape. However, the ϕ-curve of the duplex ceramic is different from that of the alumina and alumina-based duplex materials shown in Figs 5 and 7, as initially it has a negative value. This is because the ϕ-function defined by eqn (5) considers only the crack interface bridging. If microcracking in front of the crack tip is not as important as bridging, as in the case of the alumina, ϕ is greater than zero. However, if there is extensive microcracking before the propagation of a main crack, as in the case of the duplex ceramic,[13] ϕ starts with a negative value. This is because microcracking has effectively reduced the stiffness of the duplex ceramic. After some crack extension, the bridging influence exceeds the influence of microcracking and ϕ becomes positive, as shown in Fig. 8.

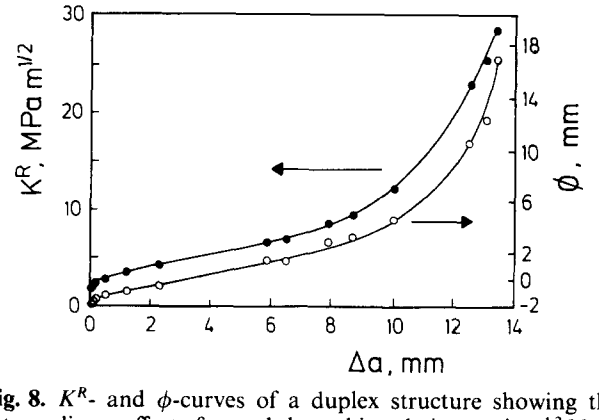

Fig. 8. K^R- and ϕ-curves of a duplex structure showing the extraordinary effect of a crack-branching chain reaction.[13] Note ϕ starts at -2, indicating that some microcrack damage occurred before the main crack growth.

It is difficult to estimate the plateau of the K^R-curve for the duplex ceramic. However, the ϕ-curve of the duplex ceramic provides a hint to the problem. If bridging stresses decrease with crack opening, the softening index n in eqn (1) must be greater than zero. The definition of the ϕ-function in eqn (5) suggests that $\phi < \Delta a$ for valid ϕ-measurements. Let it be assumed that the maximum influence of microcracking in the ϕ-function of the duplex ceramic is -2 mm, following the ϕ-curve in Fig. 8. Then, for the last three ϕ-measurements, $\phi + 2 > \Delta a$. Therefore, the ϕ-curve for $\Delta a > 12$ mm has lost its physical meaning. Since valid K^R- and ϕ-curves reach their plateau at the same crack extension as shown for the alumina in Fig. 5, the ϕ-curve of the duplex ceramic suggests that the artificial rise of the K^R-curve due to high frictional forces in the damage zone starts at about 10–12 mm crack extension and that a plateau value should have been reached for this crack length.

Let it be assumed that the lower and upper bounds for the fully saturated bridging zone X in the duplex ceramic are 8 and 10 mm respectively. From Fig. 8 it is obtained that $K_\infty = 9$ MPam$^{1/2}$ and $\phi_\infty + 2 = 5$ mm for the lower bound, and $K_\infty = 13$ MPam$^{1/2}$ and $\phi_x + 2 = 6$ mm for the upper bound. From $X/(n+1) = \phi_x + 2$, $n = 0{\cdot}6$–$0{\cdot}8$.

From eqn (3), $G_f = 303$ to 650 N/m with $\nu = 0{\cdot}2$ and $E = 244$ GPa.[38] If the crack surfaces of the duplex ceramic remain straight, $w_c = 27$–38 μm from the load and load point displacement curve.[13] Then, the maximum bridging stress $\sigma_m = 18$–29 MPa. On average, $\sigma_m = 24$ MPa, $n = 0{\cdot}7$ and $w_c = 33$ μm. It should be mentioned that the fairly large w_c value is due to the extensive process zone developed in the duplex ceramic, which is about 5 mm wide.[13] Both the significant microcracking and the dilative strain within the process zone contribute to the critical

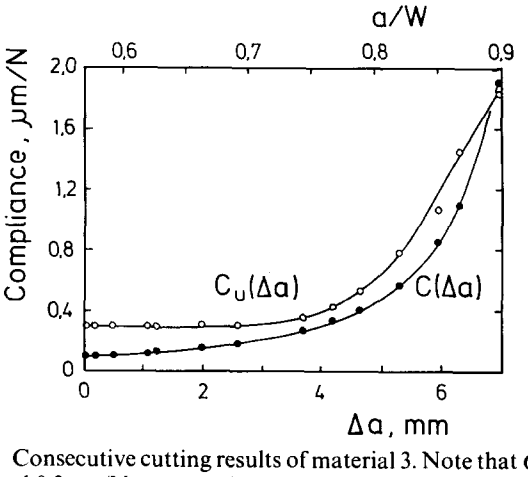

Fig. 9. Consecutive cutting results of material 3. Note that $C_u(a)$ is around 0·3 μm/N compared to $C(a)$ (= 1·8 μm/N) indicated by the intersection of the two curves.

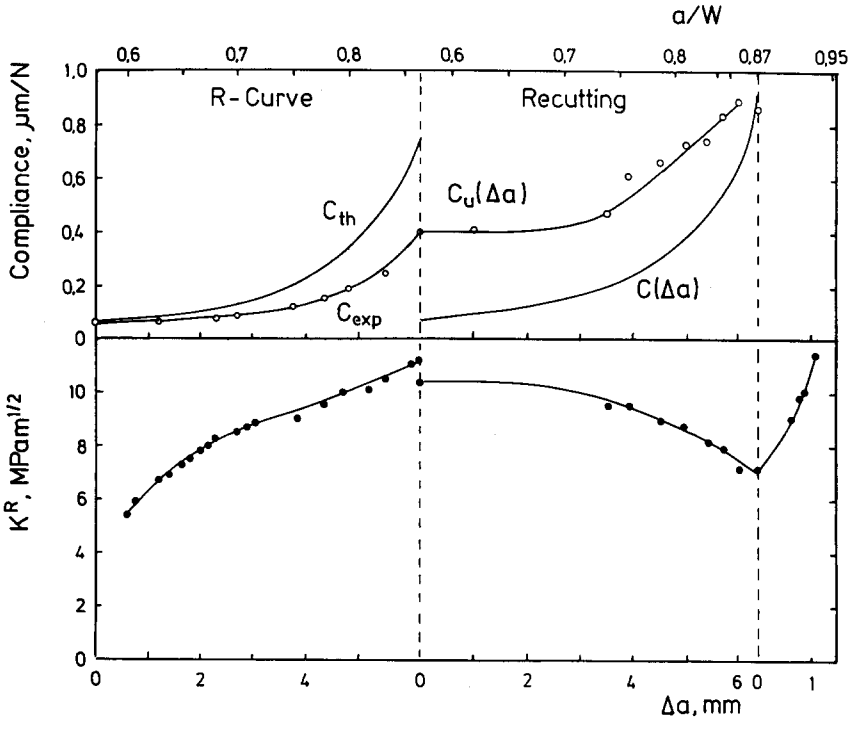

Fig. 10. K^R- and compliance curves measured during crack propagation and subsequent recutting the extended crack with material 2. As K^R increases upon crack propagation the difference between the (smaller) experimentally determined compliance and the (larger) theoretically predicted compliance gradually increases, due to the developing bridging zone. During progressive cutting K^R is reduced and the experimental compliance increases because of the removal of bridging stresses.

crack opening w_c associated with the cohesive crack model shown in Fig. 2(a).

The critical stress σ_m^c to nucleate the process zone in the duplex ceramic is about 22 MPa from an independent different approach.[13] This value is very close to the averaged maximum bridging stress determined in this study.

The consecutive cutting results of Figs 9 and 10, similar to that in Fig. 1, also suggest that bridging is the major toughening mechanism in the alumina-based duplex ceramics. On the left hand side of Fig. 10 the development of the compliance, C_{exp}, measured during crack extension is compared with the theoretical value, C_{th}. The divergence between these curves is reflected in the calculated increase of K^R with crack extension. On the right hand side the measured compliance during recutting, $C_u(\Delta a)$, is compared with the theoretical compliance, $C(\Delta a)$, which would be obtained by notching an uncracked linear–elastic-behaving material in the same way, or simply by driving a crack through the material. Notice that the measured compliance begins to increase after about 3·7 mm of notching, which indicates that the bridging zone length is about 3 mm. It is also apparent that the K^R-value, as determined from incremental crack extension during renotching, begins to fall as the bridging zone is cut. Even after renotching to about 50 μm behind the crack tip the obtained K^R-value is surprisingly still about 1·8 MPam$^{1/2}$ higher than the starting value of the K^R-curve. It is not clear whether this is caused by a contribution of effects in front of the crack tip. Immediately after the renotching procedure the crack was again extended. The corresponding K^R-values show a steep rise, similar to the behaviour observed by Steinbrech and coworkers[4,16,17] with deeply notched alumina samples.

The double-notching experiment[16] shows qualitatively the bridging influence. The successive cutting experiments initiated in previous work[22–25] can quantitatively determine the bridging stresses and their influence upon the toughness. The results in Figs 9 and 10 clearly indicate that the crack length a cannot be determined through the conventional compliance method.

5 Conclusions

A simple compliance approach has been applied to alumina ceramics of different grain size and three duplex ceramics. The technique utilizes the difference between the theoretical compliance calculable for a traction-free crack of known size and the compliance with the bridging influence measured in experiment. A so-called ϕ-function can be derived from those two compliances which provides significant information about the maximum bridging stress and the bridging stress distribution of the materials. Since the ϕ-function is based purely on bridging, a non-negative ϕ-curve is a direct proof for a bridging toughening mechanism, as in the case for alumina. On the other hand, a partially negative ϕ-curve suggests a mix of bridging and microcracking

toughening mechanisms, as in the case of the duplex ceramic, which exhibits the unusual effect of a crack-branching chain reaction.

More accurate information about the distribution and influence of bridging stresses are obtained by successively renotching the extended crack after *R*-curve testing and measuring the change in compliance and toughness.

Acknowledgements

H. E. Lutz would like to thank the Deutsche Forschungsgemeinschaft for the financial support under Contract No. lu 416/1-1.

References

1. Marshall, D. B. & Ritter, J. E., Reliability of advanced structural ceramics and ceramic matrix composites—a review. *Ceram. Soc. Bull.*, **66** (1987) 309–17.
2. Ritchie, R. O., Mechanisms of fatigue crack propagation in metals, ceramics and composites: role of crack tip shielding. *Mat. Sci. Eng.*, **A103** (1988) 15–28.
3. Hübner, H. & Jillek, W., Sub-critical crack extension and crack resistance in polycrystalline alumina. *J. Mat. Sci.*, **12** (1977) 117–25.
4. Knehans, R., Steinbrech, R. & Schaarwächter, W., Increase of crack resistance during slow crack growth in Al_2O_3 bend specimens. *J. Mat. Sci.*, **18** (1983) 265–70.
5. Swain, M. V. & Hannink, R. H. J., *R*-Curve behaviour in zirconia ceramics. In *Advances in Ceramics, Vol. 12, Science and Technology of Zirconia II*, ed. N. Claussen, M. Ruehle & A. H. Heuer. Plenum Press, New York, 1984, pp. 225–39.
6. Sakai, M. & Bradt, R. C., The crack growth resistance curve of non-phase transforming ceramics. *J. Ceram. Soc. Jpn Inter. Edn*, **96** (1988) 779–87.
7. Evans, A. G. & Faber, K. T., Crack growth resistance curve of non-phase transforming ceramics. *J. Am. Ceram. Soc.*, **67** (1984) 255–60.
8. McMeeking, R. M. & Evans, A. G., Mechanisms of transformation toughening in brittle materials. *J. Am. Ceram. Soc.*, **65** (1982) 242–6.
9. Marshall, D. B. & Swain, M. V., Crack resistance curve in magnesia-partially stabilized zirconia. *J. Am. Ceram. Soc.*, **71** (1988) 399–407.
10. Rose, L. R. F. & Swain, M. V., Two *R*-curves for partially stabilized zirconia. *J. Am. Ceram. Soc.*, **69** (1986) 203–7.
11. Evans, A. G., The new high toughness ceramics. In *Material Science Research*, Vol. 21, ed. J. A. Pask & A. G. Evans. Plenum Press, New York, 1987, pp. 775–94.
12. Faber, K. T. & Evans, A. G., Crack deflection processes—I. Theory. II. Experiment. *Acta Met.*, **31** (1983) 565–84.
13. Lutz, H. E., Claussen, N. & Swain, M. V., K^R-Curve behavior of duplex-ceramics. *J. Am. Ceram. Soc.*, **74** (1991) 11–18.
14. Marshall, D. B., Evans, A. G. & Drory, M., Transformation toughening in ceramics. In *Fracture Mechanics of Ceramics*, Vol. 6, ed. R. C. Bradt, A. G. Evans, D. P. H. Hasselman & F. F. Lange. Plenum Press, New York, 1983, pp. 289–307.
15. Rice, R. W. & Freiman, S. W., Grain-size dependence of fracture energy in ceramics—I, II. *J. Am. Ceram. Soc.*, **63** (1981) 345–54.
16. Knehans, R. & Steinbrech, R. W., Memory effect of crack resistance during slow crack growth in notched Al_2O_3 bend specimens. *J. Mater. Sci. Lett.*, **1** (1982) 327–9.
17. Steinbrech, R., Reichl, A. & Schaarwächter, W., *R*-Curve behaviour of long cracks in alumina. *J. Am. Ceram. Soc.*, **73** (1990) 2009–15.
18. Mai, Y. W. & Lawn, B., Crack interface grain bridging as a fracture resistance mechanism in ceramics: II. Theoretical fracture mechanics model. *J. Am Ceram. Soc.*, **70** (1987) 289–94.
19. Cotterell, B. & Mai, Y. W., Modelling crack growth in fibre-reinforced cementitious materials. *Mater. Forum*, **11** (1988) 341–51.
20. Foote, R. M. L., Mai, Y. W. & Cotterell, B., Crack growth resistance curves in strain-softening materials. *J. Mech. Phys. Solids*, **34** (1986) 593–607.
21. Swain, M. V., *R*-Curve behaviour in a polycrystalline alumina material. *J. Mater. Sci. Lett.*, **5** (1986) 1313–15.
22. Hu, X. Z. & Wittmann, F. H., Fracture process zone and K_r-curve of hardened cement paste and mortar. In *Fracture of Concrete and Rock: Recent Developments*, ed. S. P. Shah, S. E. Swartz & B. Barr. Elsevier, London, 1989, pp. 307–16.
23. Hu, X. Z., Fracture process zone and strain-softening in cementitious materials. Report No. 1, Institute for Building Materials, Swiss Federal Institute of Technology, Zurich, 1989.
24. Hu, X. Z. & Wittmann, F. H., An analytical method to determine the bridging stress transferred within the fracture process zone. *Cement and Concrete Research*, (1991) in press.
25. Hu, X. Z. & Wittmann, F. H., Experimental method to determine extension of fracture process zone. *J. Mater. Civil Engineering*, **2** (1990) 15–23.
26. Hu, X. Z. & Mai, Y. W., A general method for determination of crack-interface bridging stresses. *J. Mater. Sci.*, in press.
27. Hu, X. Z., Lutz, H. E. & Swain, M. V., Crack tip bridging stresses in ceramic materials. *J. Am. Ceram. Soc.*, in press.
28. Lutz, H. E. & Swain, M. V., Interrelation between flaw-resistance, *R*-curve behavior, and thermal shock behavior in ceramics. *J. Am. Ceram. Soc.*, in press.
29. Lutz, H. E. & Claussen, N., Duplex-ceramics: I. Stress calculations, fabrication and microstructure. *J. Eur. Ceram. Soc.*, **7** (1991) 209–18.
30. Lutz, H. E. & Claussen, N., Duplex-ceramics: II. Strength and toughness. *J. Eur. Ceram. Soc.*, **7** (1991) 219–26.
31. Lutz, H. E., Swain, M. V. & Claussen, N., Thermal shock behavior of duplex-ceramics. *J. Am. Ceram. Soc.*, **74** (1991) 19–23.
32. ASTM Designation E 399–81, 1981 Annual Book of ASTM Standards, Part 10, American Society for Testing and Materials, Philadelphia, PA.
33. Freiman, S. W., Mulville, D. R. & Mast, P. W., Crack propagation in brittle materials. *J. Mat. Sci.*, **8** (1973) 1527–33.
34. Kanninen, M. F., *Int. J. Fract.*, **9** (1973) 83–91.
35. Saxena, A. & Hudak, S. J., *Int. J. Fract.*, **14** (1978) 453–67.
36. Rodel, J., Kelly, J. F. & Lawn, B. R., In-situ measurements of bridged crack interfaces in the SEM. *J. Am. Ceram. Soc.*, **73** (1990) 3313–18.
37. Lawn, B. R., Fundamental condition for the existence of microcrack clouds in monophase ceramics. *J. Eur. Ceram. Soc.*, **7** (1991) 17–20.
38. Lutz, H. E., Aufbau und Eigenschaften von Al_2O_3- und ZrO_2-Keramiken mit kugeligen Druckzonen. PhD These, Hamburg-Harburg, 1989.

Appendix: Derivation of the ϕ-Function

If $w_c/X \ll 1$, a linear crack profile can be assumed within the bridging zone as shown in Fig. 2(a).

$$\frac{w}{w_c} = \frac{x}{X} \tag{A1}$$

For convenience, the power-law bridging stress function[18,20] and the fracture energy are also given.

$$\frac{\sigma_b}{\sigma_m} = \left[1 - \frac{w}{w_c}\right]^n \tag{A2}$$

$$G_f = \frac{\sigma_m w_c}{n+1} \tag{A3}$$

For a bridged crack in Fig. 2(a), $C(a)$ and $C_u(a)$ can be determined. Let $C_u(x)$ denote the measured compliance after the initial notch a_0 is extended by renotching to position x in Fig. 2(a). Obviously, $C_u(0) = C(a)$ if $x = 0$. It has been proven in previous work[22-24] that the bridging stress $\sigma_b(x)$ at position x is given by:

$$\frac{\sigma_b(x)}{\sigma_m} = -\frac{C^2(a)}{C'(a)} \cdot \frac{C_u'(x)}{C_u^2(x)} \tag{A4}$$

where $C'(a) = dC(a)/da$ and $C_u'(x) = dC_u(x)/dx$, and that before renotching, for Fig. 2(a),

$$\frac{C(a)}{C'(a)} \cdot \left\{\frac{C(a)}{C_u(a)} - 1\right\} = X \cdot \frac{G_f}{\sigma_m w_c} \tag{A5}$$

In eqns (A4) and (A5) $C_u(a)$ is the measured compliance before renotching, while $C_u(x)$ is the compliance measurement after the initial notch has been extended to position x shown in Fig. 2(a). If the compliance $C_u(x)$-curve (or $C_u(\Delta a)$-curve in Fig. 1) is measured experimentally, the bridging stress $\sigma_b(x)$ can be solved through eqns (A4) and (A5).

By substituting eqns (A1) and (A2) into eqn (A4), one obtains

$$-\frac{C^2(a)}{C'(a)} \cdot \frac{dC_u(x)}{C_u^2(x)} = \left[1 - \frac{x}{X}\right]^n dx \tag{A6}$$

Before the bridging zone is fully saturated, bridging stresses exist over the whole crack extension $\Delta a (= a - a_0)$. As x can vary from 0 to Δa (from the crack tip a to the initial notch tip a_0), eqn (A6) can be integrated for $0 < x < \Delta a$ and $C(a) > C_u(x) > C_u(a)$. Hence,

$$\frac{C(a)}{C'(a)} \cdot \left\{\frac{C(a)}{C_u(a)} - 1\right\} = \frac{X}{n+1} \cdot \left\{1 - \left[1 - \frac{\Delta a}{X}\right]^{n+1}\right\} \tag{A7}$$

where $C_u(a)$ is simply the compliance measured without renotching. Let ϕ represent the left hand side of eqns (A5) or (A7). From eqns (A3), (A5) and (A7) one obtains

$$\phi = \frac{C(a)}{C'(a)} \cdot \left\{\frac{C(a)}{C_u(a)} - 1\right\} = \begin{cases} \dfrac{X}{n+1} & \Delta a > X \\ \dfrac{X}{n+1} \cdot \left\{1 - \left[1 - \dfrac{\Delta a}{X}\right]^{n+1}\right\} & \Delta a < X \end{cases} \tag{A8}$$

Insofar as the exponent n is concerned, renotching is no longer necessary. From the measurements of the crack a and compliance $C_u(a)$, a ϕ-curve can be established with eqn (A8). Then, the steady-state bridging zone X and the exponent n of the power-law bridging stress distribution can be determined. Full details of the compliance analysis on $C_u(a)$ and $C(a)$ can be found in Refs 22–24.